Proposal 20170876

Title
Water feature detectability in subsecond XTM of gas diffusion layer of PEFC

Abstract
Water management is crucial to the performance of polymer electrolyte membrane fuel cell (PEFC). To realize the 4D water visualization in operando PEFC condition, X-ray tomographic (XTM) imaging is a powerful tool. Tracking the fast water dynamics requires high temporal resolution XTM with scan time in the sub-second range. The proposed experiment aims to quantify the influence of varying imaging parameters on water feature detectability inside the gas diffusion layer (GDL) used in PEFC, which is prerequisite for future subsecond XTM of PEFC.

Proposer / Spokesperson	
Mr. Hong Xu	Allgemeine Energie (ENE), Paul Scherrer Institut hong.xu@psi.ch

Principal investigator	
Dr. Jens Eller	Allgemeine Energie (ENE), Paul Scherrer Institut

Co-Proposer	
Dr. Felix N Buechi	Allgemeine Energie (ENE), Paul Scherrer Institut
Mrs. Minna Bührer	Photon Science (PSD), Paul Scherrer Institut

Experiment Category	
Experiment Type	Normal
Research Area	Catalytic Materials/Surface Science

Experiment Requirements	
Eligible for EU Support	No
Number of Shifts Required	6
Beamline/Station	TOMCAT

Links to related proposals of relevance to the current proposal			
Proposal	Title/Proposer/Infos given by the proposer about the relation		Report
20120161	Title: Proposer:	XTM imaging of water and ice in the porous structures of Fuel Cells Dr. Felix N Buechi	Available
20140327	Title: Proposer:	XTM imaging of PEFC start-up at sub-zero temperatures Dr. Felix N Buechi	Available

A Goals

Operando X-ray tomographic imaging (XTM) is a powerful technique, able to image the liquid water in PEFCs on the scale of gas diffusion layer (GDL) pores with pixel sizes of 2 to 3 micrometers. However, today the fastest *operando* XTM scans of realistic cells require acquisition times of about 5-10 s, limiting the technique to investigation of stationary operation conditions [1,2]. **Our aim is to reduce the scanning time by two orders of magnitude** vs. state of the art to 0.1s (or even below) for a 3D-volume that will allow insights into dynamics of the liquid phase that are expected to dominate during transient PEFC operation. This requires the exploitation of advanced reconstruction techniques and image-processing approaches that allow to identify the liquid water phase in the 3D-images from low signal to noise CT data. In order to have confidence on the identified water distribution, it is **essential to quantify consequences of the reduced scan time** on the spatial resolution and feature detectability.
Therefore, the **proposed experiments aim to quantify** the influence of varying imaging parameters (scan time, poly/mono-chromatic beam, contrast mode, reconstruction methods) on the **capability to resolve the individual water clusters** inside the GDL.

B Background

Hydrogen fed polymer electrolyte fuel cells (PEFC) are expected to play a major role in a future decarbonized energy system, in particular in the mobility sector. Water management is the major limiting factor in PEFC for further increasing power density. Inside the PEFC, the water management is complex: on one hand, the membrane needs a certain hydration state in order to ensure sufficient proton conductivity; on the other hand, excessive water leads to blocked gas pathways in the porous structures with increased mass transport losses. Product water is transported in liquid state by capillary forces or in the vapor phase by diffusion and convection from the catalyst layer through the GDL towards the gas flow channels, in opposite direction of the oxygen diffusion towards the catalyst layer (see Fig. 1). Under high current densities, necessary for high power densities, the water production rate becomes high and the volume occupied by water can dramatically decrease the accessibility of oxygen, resulting in mass transport limitations (so-called flooding). In vehicles and other demanding applications the fuel cell is operated in non-steady state mode, following a transient load profile. This requires a fast characterization technique for understanding of the transient water transport in the GDL..

While XTM has proven a powerful technique to gain understanding of the structure-property relationship of gas and liquid water transport in the GDL at static conditions [1-3] with signal-to-noise ratios of about 6 and higher. Recent progress in the image processing pipeline of PEFC XTM data has opened the door to image the dynamics of the water distribution (see Fig. 2) at reduced signal-to-noise ratios (SNR; see Fig. 3) with simplified cells [4]. For boundary-bias free analysis of the water distribution in a channel-rib repetitions unit a more realistic double channel cell is essential (see Fig. 4a). Preliminary experiments have shown, that for this more realistic cell design even lower SNR values have to be expected.

A precise quantification of the feature detectability of water distribution acquired by the available sub-second XTM capabilities at TOMCAT is required in advance to future operando experiments.

C Experimental method; specific requirements

As the fluctuating water distribution in the GDL pores is challenging to reference and compare for scans acquired at times an indirect quantification is required. It will be implemented in two steps: 1) In a **first campaign** it is planned to fill the gas channels of one flow field of the operando cell (see Fig. 4a) with liquid water and use the bulk water and void domains in the channels to calculate the contrast-to-noise (CNR) ratio between water and void. This simple **ex-situ experiment used to screen a wide range of imaging parameters** (scan time, poly/mono-chromatic beam, contrast mode, reconstruction methods). 2) In **second campaign**, the two energy conditions with the **best CNR** ratios will be **studied in detail with realistic water distributions** of operating fuel cells. Therefore the water distribution will be **fixed by freezing** such that multiple scan with the same water distribtion will be possible. The operando PEFC setup with a compact cooling system (see Fig. 4b-c; developed for proposal 20140327) will be used, which enables the capability to freeze the cell down to -20°C. As the density of ice is lower than of water, the CNR and structure similarity comparison are regarded as slight underestimation of the image quality for operando conditions with liquid water.
Coherent synchrotron radiation is needed to record absorption and phase contrast XTM images at the TOMCAT beamline (X02DA) using the fast tomographic setup (Gigafrosty camera and 4-fold macroscope).

D Results expected

The detailed characterization of the contrast-to-noise and feature detectability will provide the confidence to exploit the sub-second XTM capabilities of TOMCAT for future studies of the dynamics of the water distribution in the GDL of PEFCs under transient load conditions. This will enable an ultimative understanding of the coupling of power limitations at transient PEFC operation with liquid water dynamics at the pore scale level and thanks to the increased number of scans, the redistribution of the water phase over various timescales will become accessible.

E Estimate and justification of the beamtime

To study the **bulk water-void CNR in campaign 1** for the influence of the scan time (8 settings, 0.05 to 10 s; requiring 1 h) and for the influence of number of projections and exposure time at fixed scan time (5 scan times (0.05 to 1 s) with each 5 combinations of projections (20 to 1000) and exposure time (0.5 to 10 ms); requiring 2 h) at 6 different X-ray beam settings (mono-chromatic (11 keV, 13.5 keV, 16 keV, 18.5 keV, 21 keV) and polychromatic (5% power) requiring together with beamline (4h) and setup preparation (2h) **24h** (3 shifts). To study the f**eature detectability in campaign 2** will repeat the scan time variations (1 h) and a simplified variation of number of projections and exposure time at fixed scan time (1.5 h) at two energy settings. These experiments will require together with acquisition of dry structure reference scans (1h), cell mounting (2 h), beamline (4h) and setup preparation (2h) for two repetitions **24h** (3 shifts). In **total 48 h** (6 shifts) are requested.

F References relevant to the experiment description

[1] I. Mayrhuber et al., Chem. Electrochem. 2015.
[2] J. Eller, J. Roth, F. Marone, M. Stampanoni and F. N. Büchi, “Operando properties of gas diffusion layers: saturation and liquid permeability.” J. Electrochem. Soc. 164(2), 115-126, 2017.
[3] T. Rosén, J. Eller, J. Kang, N.I. Prasianakis, J. Mantzaras, F.N. Büchi, “Saturation Dependent Effective Transport Properties of PEFC Gas Diffusion Layers,”J. Electrochem. Soc. 159, F536-F544, 2012.
[4] J. Eller, F. Marone and F. N. Büchi, “Operando sub-second tomographic imaging of water in PEFC gas diffusion layers.” ECS Trans. 69(17), 523–531, 2015.

SLS related publications of the proposers (within the last 18 months)
[1] J. Eller, J. Roth, F. Marone, M. Stampanoni, F.N. Buechi; Operando properties of gas diffusion layers: Saturation and liquid permeability; J. Electrochem. Soc. 164 (2), F115-F126 (2017). [2] A. Forner-Cuenca, J. Biesdorf, A. Lamibrac, V. Manzi-Orezzoli, F.N. Büchi, L. Gubler, T.J. Schmidt, P. Boillat; Advanced water management in PEFCs: Diffusion layers with patterned wettability: II. Measurement of capillary pressure characteristic with neutron and synchrotron imaging; J. Electrochem. Soc. 163 (9), F1038-F1048 (2016). [3] I. V. Zenyuk, A. Lamibrac, J. Eller, D. Y. Parkinson, F. Marone, F. N. Buechi and Adam Z. Weber; Investigating Evaporation in Gas Diffusion Layers for Fuel Cells with X-ray Computed Tomography; J. Phys. Chem. C, 120 (50), F28701–F28711 (2016). [4] T. Agaesse, A. Lamibrac, F. N. Buechi, J. Pauchet, M. Prat; Validation of pore network simulations of ex-situ water distributions in a gas diffusion layer of proton exchange membrane fuel cells with X-ray tomographic images; J. Power Sources, 331, F462-F474 (2016). [5] A. Lamibrac, J. Roth, M. Toulec, F. Marone, M. Stampanoni and F. N. Buechi; Characterization of Liquid Water Saturation in Gas Diffusion Layers by X-Ray Tomographic Microscopy; J. Electrochem. Soc. 163(3), F202-F209 (2016). [6] S. H. Eberhardt, F. Marone, M. Stampanoni, F. N. Buechi and T. J. Schmidt; Operando X-ray Tomographic Microscopy Imaging of HT-PEFC: A Comparative Study of Phosphoric Acid Electrolyte Migration; J. Electrochem. Soc. 163(8), F842-F847 (2016). [7] P. Pietsch, D. Westhoff, J. Feinauer, J. Eller, F. Marone, M. Stampanoni, V. Schmidt and V. Wood; Quantifying microstructural dynamics and electrochemical activity of graphite and silicon-graphite lithium ion battery anodes; Nature Communications, 7, 12909 (2016). [8] J. Eller, F. Marone, and F.N. Buechi, Operando Sub-Second Tomographic Imaging of Water in PEFC Gas Diffusion Layers, ECS Transactions, 69, 523-531 (2015). [9] S. H. Eberhardt, F. Marone, M. Stampanoni, F. N Buechi and T. J. Schmidt; Imaging Phosphoric Acid Migration in High Temperature Polymer Electrolyte Fuel Cells by X-Ray Tomographic Microscopy; ECS Trans. 69(17), F591-599 (2015).

Other publications of the proposers (within the last 18 months)
[1] L. Holzer, O. Pecho, J. Schumacher, Ph. Marmet, O. Stenzel, F.N. Buechi, A. Lamibrac, B. Muench; Microstructure-property relationships in a gas diffusion layer (GDL) for Polymer Electrolyte Fuel Cells, Part I: effect of compression and anisotropy of dry GDL; Electrochimica Acta, 227 F419-434 (2017). [2] M. Suermann, T.J. Schmidt, F.N. Buechi; Cell performance determining parameters in high pressure water electrolysis; Electrochim. Acta, 211, 989-997 (2016). [3] P. Pietsch, M. Hess, W. Ludwig, J. Eller, and V. Wooda; Combining operando synchrotron X-ray tomographic microscopy and scanning X-ray diffraction to study lithium ion batteries; Sci Rep. 6, F27994 (2016). [4] M. Suermann, T. J. Schmidt and F. N Buechi; Investigation of Mass Transport Losses in Polymer Electrolyte Electrolysis Cells; ECS Trans. 69(17), F1141-1148 (2015).

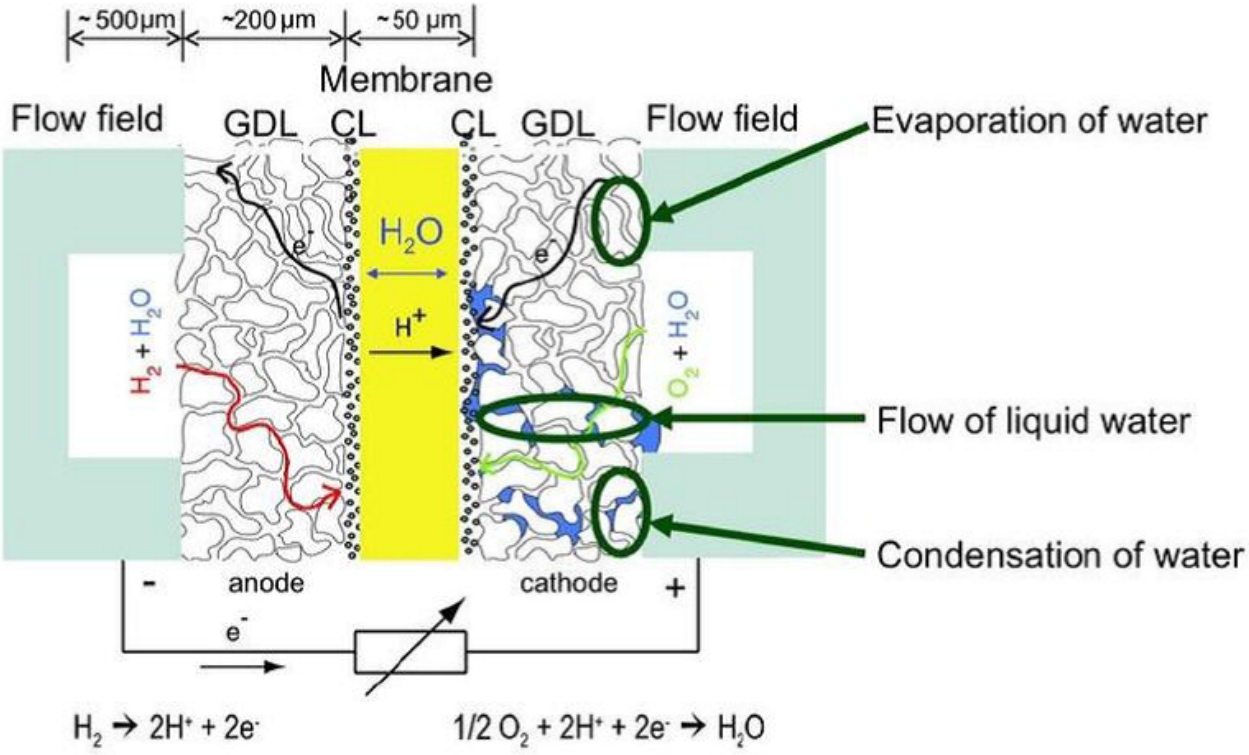

Figure 1: PEFC working principle and water distribution modes

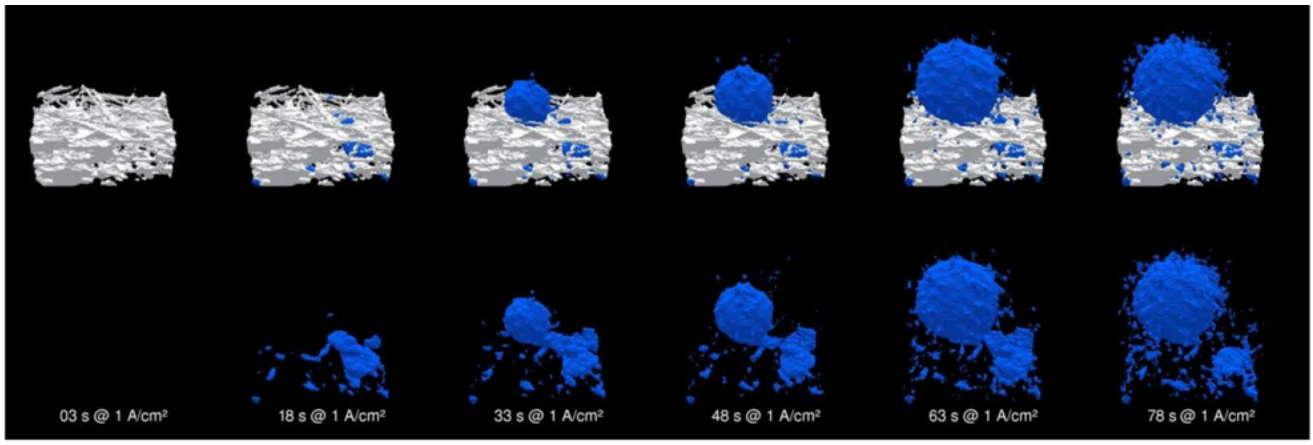

• Surface rendering of the liquid water for selected scans. In the top row, the liquid water is shown together with the solid GDL, while the GDL is not shown in the bottom row; droplet is not removed due to low gas speed (approx. 0.8 m/s).

Figure 2:

a)

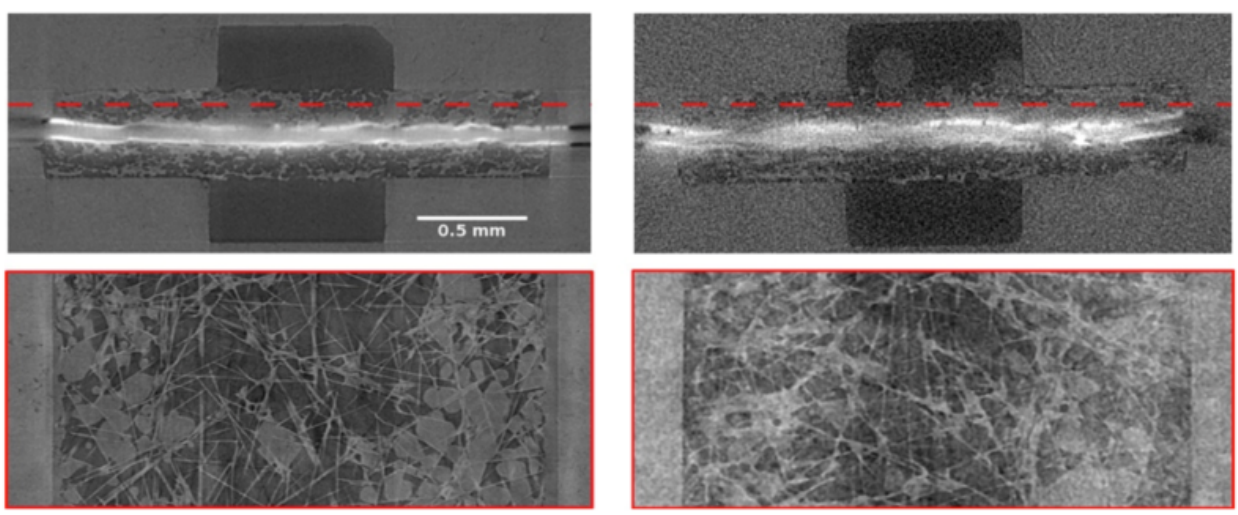

- Comparison of 8 s scan (left) and a feasibility study test scan of 0.75 s right of the simplified (single-channel) cell. Top row: Tomographic 'through-plane' slices that allow an snapshot comparison of the anode and cathode saturation; the dashed red line marks the position of an 'in-plane' section within the cathode GDL (bottom row).

b)

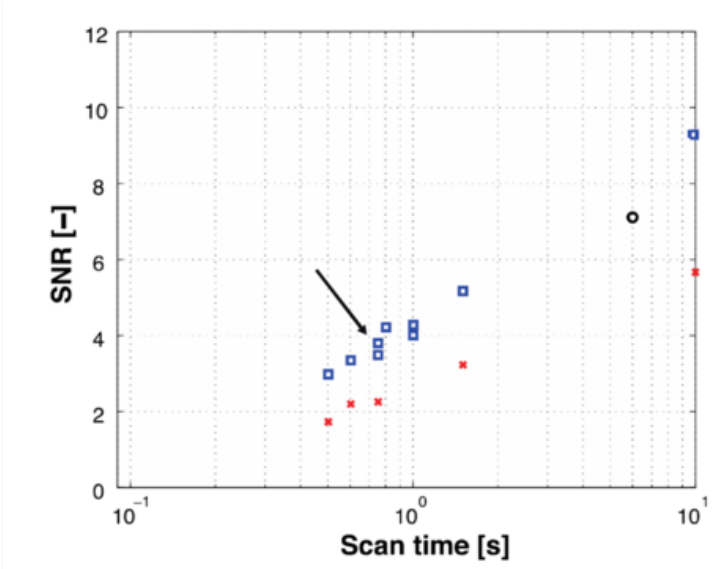

- Comparison of CNR values for different scan times for a simplified cell (blue squares) and realistic cells (red cross and black circle). Beam energy was 13.5 keV for scans marked with blue squares or red cross, and 16 keV for the scan labeled with a black circle; arrow denotes settings used for the presented data.

Figure 3:

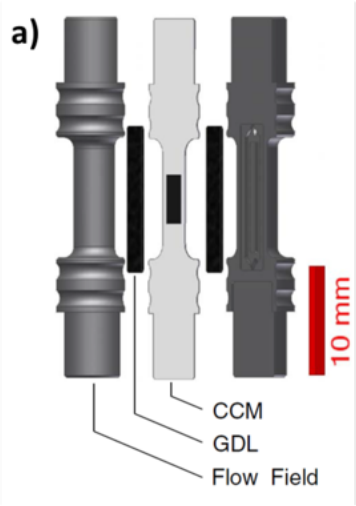

a) Schematics of XTM fuel cell.

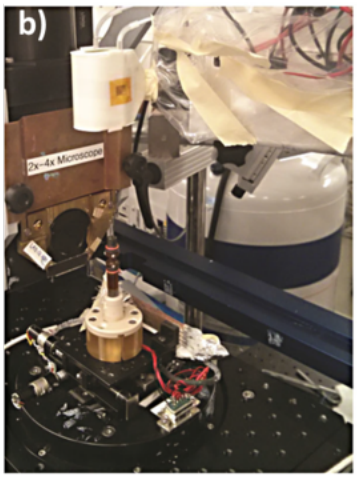

b) Freezing setup at the beamline in front of the scintillator (X-ray beam coming from the right side).

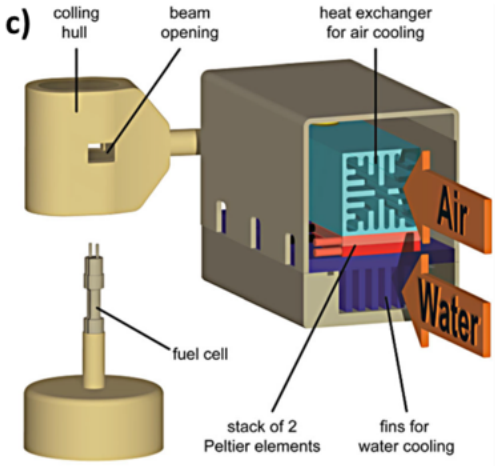

c) Schematic illustration of the freezing setup; the cooling hull is lowered over the cell, which is then cooled by a cold air stream.

Figure 4:

Sample

Sample #1

Sample and chemical substance to be used in this experiment	
Substance	Carbon Fiber; Platinum contained catalyst
Chemical formula	Carbon fiber paper surface-treated with PTFE or FEP; Platinum contained catalyst
Structure	Multilayer
Size X	5
Size Y	5
Size Z	0.2
Mass	1.6
Container	Vespel cell
High purity	No
After the experiment the sample will be	Removed by user
No ethical issues declared on this sample.	

Sample environment	
Cryojet [K]	240-370
Hotair blower	No
Special environment	Compact cooling system will be used for freezing fuel cell.
High voltage	No
High pressure	No
High temperature	No
Magnetic field	No
Cryogenic liquid	No
Be window	No

Safety aspects	
Chemical hazards	
Chemical hazards	Burnable chemicals and solvents Explosive Gases (CO, H2, N2, O2, CO2, noble gases, others) Reactive chemicals
Specification of chemical hazards	In the steup, for running the fuel cell, the sample is overflowed with synthetic air or hydrogen with low gas flow up to 200ml/min.

Experimental report of related proposal 20120161

You have linked proposal 20120161 as previous proposal with relevance to the current one.
Since you are not on the authorlist of 20120161 the content of the experimental report
is for confidentiality reasons not shown here.

The members of the review committee will see the actual report in their version of the PDF.

Experimental report of related proposal 20140327

You have linked proposal 20140327 as previous proposal with relevance to the current one.
Since you are not on the authorlist of 20140327 the content of the experimental report
is for confidentiality reasons not shown here.

The members of the review committee will see the actual report in their version of the PDF.

Experimental Report

Water feature detectability in subsecond XTM of gas diffusion layer of PEFC

Hong Xu, Minna Bührer, Jens Eller

(Proposal 20170876)

Overview

The scheduled beamtime on 18th Sept 2017 was dedicated to study the influences by decreasing the XTM scan time towards 0.1 s, which paves the way for 4D XTM imaging of the transient water distribution in the gas diffusion layer (GDL) during polymer electrolyte fuel cell (PEFC) operation. Variations of different imaging parameters (beam energy, scan time) are presented and their consequences on the Contrast-to-Noise (CNR) ratio and further on the detectability of the micro-structural water features are discussed.

Quality of measurement/data

Followed by the proposed experiment in proposal 20170876, XTM scans for a cathode water filled channel fuel cell were collected at four monochromatic beam energy levels (11 keV, 13.5 keV, 16 keV, 18.5 keV) and polychromatic beam energy with variation of scan time from 12.8s to 0.1s. Several high quality scans was taken between the group of scans for the quality checking and comparison. The reconstructed images with missing pixels mask and ring removal were sufficient for post processing and quantification.

Status and progress of evaluation

The data collected at monochromatic beam energy levels are fully reconstructed and processed as presented in the results part. For polychromatic beam data, it is still under optimization of water feature detectability by different reconstruction algorithms. The complete evaluation will be expected to finish before next scheduled beamtime.

Results

In order to improve the image quality towards subsecond X-ray tomographic microscopy, it is vital to understand the influence of imaging conditions on the image quality. The CNR(H_2O/Void) was studied for monochromatic beam energies between 11 keV and 18.5 keV with tomographic scan times ranging from 12.8 s to 0.1 s, which approaches the hardware limitation of image acquisition time 0.05 s at the TOMCAT beamline. The consequences of the time reduction for tomographic scans are shown qualitatively in Figure 1. While the void flow field channels remain visible down to a scan time of 0.1 s in the through-plane slices, the GDL structures can be only seen until 0.8 s scan time in the in-plane view. Some fiber structures are already lost at a scan time of 1.6 s.

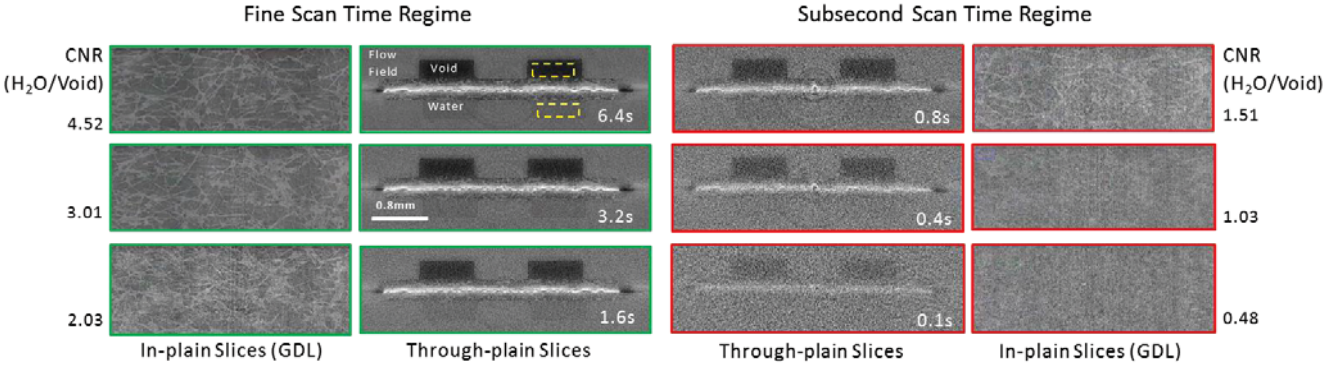

Figure 1: Tomographic in-plain slice and through-plain slice for different tomographic scan times (6.4 s, 3.2 s, 1.6 s, 0.8 s, 0.4 s, 0.1 s) at 13.5 keV; the yellow dashed rectangulars indicate the sampling domains for CNR calculation. The CNR was defined as $\mathrm{CNR}(H_2O/Void) = \frac{mean(H_2O)-mean(Void)}{\sqrt{[StdDev(H_2O)^2+StdDev(Void)^2]/2}}$.

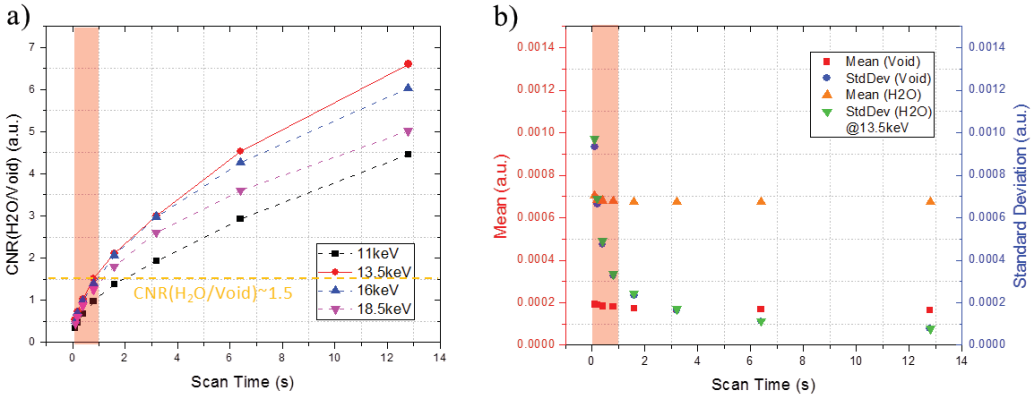

Figure 2: a) Contrast-to-noise ratio between water and void domains for different tomographic scan times at energy levels between 11 keV and 18.5 keV; b) Mean and standard deviation of the H_2O and void domains versus scan time at 13.5 keV; the red area in plot a) and b) indicates the subsecond scan time regime.

At an energy level of 13.5 keV the CNR(H_2O/Void) is the highest for all scan settings (see Figure 2 a). At the lowest energy of 11 keV the X-ray flux and the transmission are lowest and therefore the CNR is smallest for the all scan settings. The reduction of CNR for energies above 13.5 keV is due to the deceasing of the attenuation coefficient of water. For subsecond scan times below 0.8 s the CNR(H_2O/Void) reduces to below 1.5, which challenges the segmentation of the liquid water in the cell. To reveal the reason behind this, a detailed analysis of the contributions of mean and standard deviation levels to the CNR at 13.5 keV is shown in Figure 2 b. The mean gray scale value of both H_2O and void domain remains stable, as the attenuation coefficients are not affected by the scan time. The standard deviations increase as the scan time decreases, especially in the subsecond scan time regime, with similar values for the water and void domains. When the scan time reduces to 0.5 s and below, the standard deviations are almost the same as the mean level of the H_2O domain, and as the noise level reaches the signal level the CNR drops below 1.

The low CNR requires appropriate image denoising before segmentation in order to increase the detection level of the true water domains and to minimize the amount of falsely assigned water domains. Median filter (13) and anisotropic diffusion filter (14) are applied to reduce noise while preserving the edges of the water boundaries. The influence of the number of iterations of the anisotropic diffusion (AD) filter was analyzed for the noise level of 1.6 s scan time. When increasing the number of iterations, the noise in the background decreases (see Figure 3 c). The CNR between water domain and background increases from 2.2 (no AD iteration) to 7.7 (5 AD iterations), which exceeds even the CNR(H_2O/Void) of a 12.8 s scan. This leads to reduction of the falsely segmented water from almost 12 % (no AD iteration) below 1 % (5 AD iterations). The drawback of the strong filtering is a loss of feature detectability which starts already for sphere with a diameter of 10 pixels and cylinder with a diameter of 9 pixels. For larger diameter structures, the anisotropic diffusion filter increases the feature detectability. At cylinder diameters of 5-7 pixels the 5 AD iterations prior to segmentation start to show clearly lower feature detectability levels compared to fewer iterations. This effect becomes more pronounced for even smaller features. 1 pixel diameter cylinders are completely removed by 5 AD iterations, while they can be detected at least partially after 1 AD iteration. Generally, the cylindrical domains show higher feature detectability levels than the spherical domains at the same diameter, as their connectivity is higher (see Figure 3 a-b). 3 AD iterations are identified as a compromise between the detection of small diameter features and the reduction of falsely detected water in the background.

In the following feature detectability analysis, the subtracted image has therefore been filtered with a 3D median filter (radius 1 pixel) and a 3D anisotropic diffusion filter (3 iterations) before segmentation through thresholding. The influence of the scan time on the feature detectability when denoising with 3 AD iterations is presented in Figure 4. A clearly better detection level can be found

for the 3.2 s scan, where feature detectability levels of more than 80 % are observed for cylinders with diameters of 5 pixels and the amount of false water does not exceed 1 %. For the 0.4 s scan, the feature detectability is kept above 60 % with the diameter down to 4 pixels. Due to sampling the virtual water structures only once, fluctuations of feature detectability can be observed for both spherical and cylindrical water clusters with diameter below 8 pixels. Detectability level of subsecond scans needs to be improved. Further studies on threshold level as well as denoising filter combinations are needed. The application of phase retrieval and iterative reconstructions schemes are expected to improve feature detectability further.

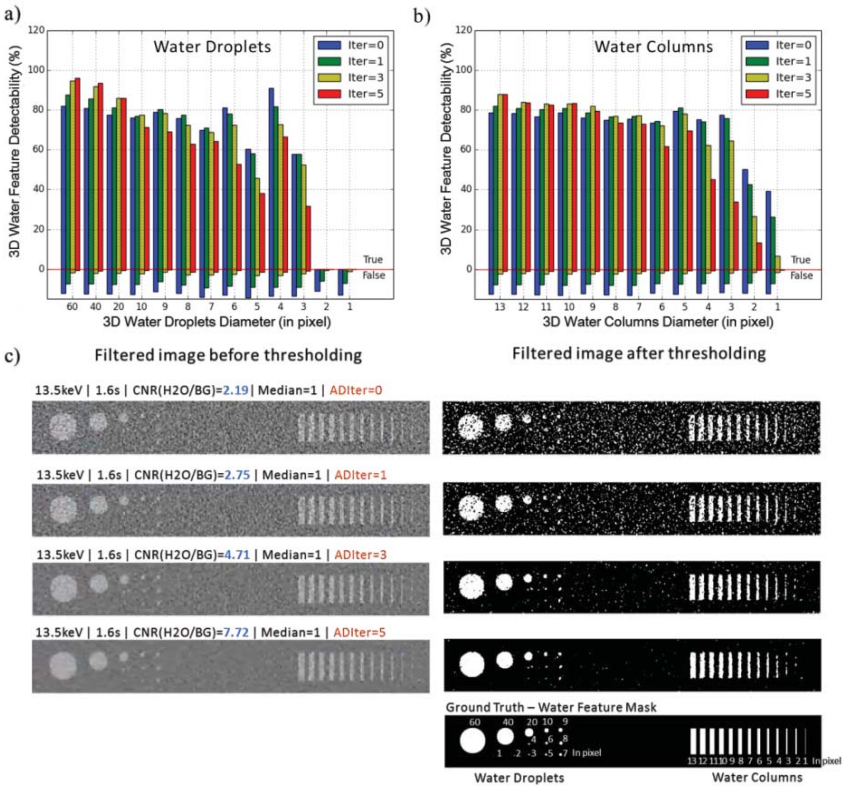

Figure 3: Feature detectability of artificial water droplets a) and water columns b) with various diameters for different number of anisotropic diffusion iterations for a tomographic scan time of 1.6 s at 13.5 keV; bar height above the red line is the percentage of true water voxels in the ground truth domain, bar height below the red line is the percentage of false voxels outside the ground truth within 10 pixels from the surface of the ground truth; c) 2D representation of 3D filtered images and the corresponding segmented images for different number of anisotropic diffusion iterations. The ground truth is shown below as a reference.

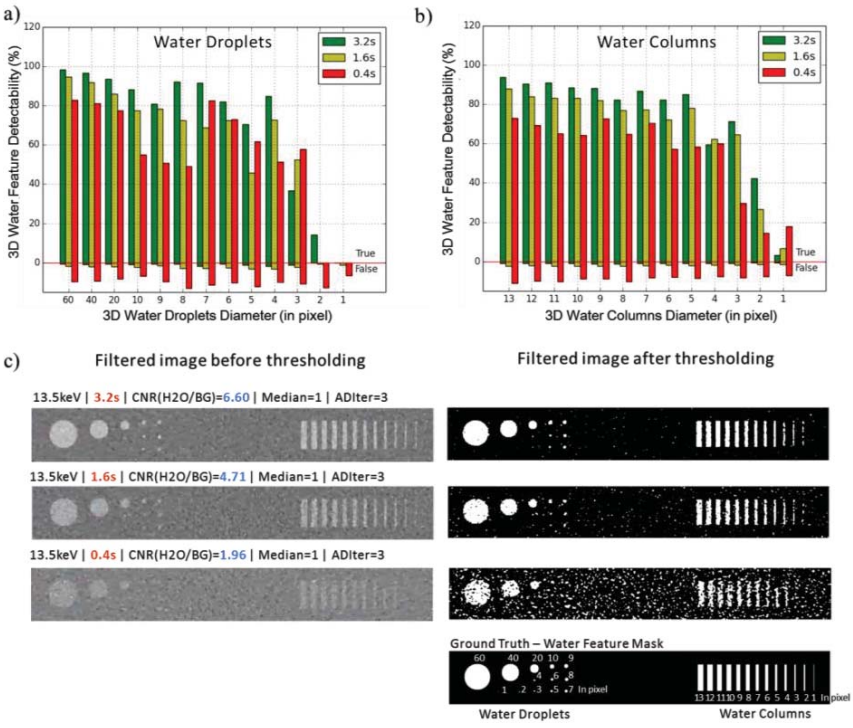

Figure 4: Feature detectability of artificial water droplets a) and water columns b) with different diameters for tomographic scan times 3.2 s, 1.6 s and 0.4 s at 13.5 keV; bar height above the red line is the percentage of true water voxels in the ground truth domain, bar height below the red line is the percentage of false voxels outside the ground truth within 10 pixels from the surface of the ground truth; c) 2D representation of 3D filtered images (left) and the corresponding segmented images (right) for scan times 3.2 s, 1.6 s and 0.4 s. The ground truth is shown below as a reference.

Publications linked to 20170876

Publications linked to this proposal
Fighting the Noise: Towards the Limits of Subsecond X-ray Tomographic Microscopy of PEFC Xu H, Bührer M, Marone F, Schmidt Thomas J, Büchi F, Eller J ECS TRANSACTIONS*80 395 (2017)* DOI : 10.1149/08008.0395ecst